Journal of Petrology, 2020, 1–17 doi: 10.1093/petrology/egaa076 Advance Access Publication Date: 17 July 2020 Original Article



Regional Quartz Inclusion Barometry and Comparison with Conventional Thermobarometry and Intersecting Isopleths from the Connecticut Valley Trough, Vermont and Massachusetts, USA

Oliver M. Wolfe* and Frank S. Spear

Department of Earth and Environmental Sciences, Rensselaer Polytechnic Institute, 110 8th Street, Troy, NY 12180, USA

*Corresponding author. Telephone: (818) 687-1186. E-mail: wolfeo2@rpi.edu

Received 19 August 2019; Accepted 9 July 2020

ABSTRACT

A comparative analysis of Raman shifts of quartz inclusions in garnet was made along two traverses across the Connecticut Valley Trough (CVT) in western New England, USA, to examine the regional trends of quartz inclusion in garnet (QuiG) Raman barometry pressure results and to compare this method with conventional thermobarometry and the method of intersecting garnet core isopleths. Overall, Raman shifts of quartz inclusions ranged from 1.2 to 3.5 cm⁻¹ over all field areas and displayed a south to north decrease, matching the overall decrease in mapped metamorphic grade. Raman shifts of quartz inclusions typically did not show systematic variation with respect to their radial position within a garnet crystal, and indicate that garnet probably grew at nearly isothermal and isobaric pressure-temperature (P-T) conditions. The P-T conditions inferred from conventional thermobarometry were in the range of \sim 500–575 °C and \sim 7.4–10.3 kbar over the sample suite and are in good agreement with previous published thermobarometry throughout the CVT. These P-T results are broadly consistent with QuiG barometry and also suggest that garnet grew isothermally and isobarically at near peak P-T conditions. However, P-T conditions and P-T paths inferred using either garnet core thermobarometry or garnet core intersecting isopleths yield results that are internally inconsistent and generally disagree with the pressure results from QuiG barometry. Garnet core isopleth intersections consistently plotted between the nominal garnet-in curve on mineral assemblage diagrams and the P-T conditions constrained by QuiG isomekes for the majority of the sample suite. Additionally, most samples' P-T results from QuiG barometry and rim thermobarometry show marked disagreement from those derived from garnet core thermobarometry, compared with the minority that showed agreement within uncertainty. Pressures calculated from QuiG barometry ranged from 8.5 to 9.5 kbar along the traverses in western Massachusetts (MA) and central Vermont (VT) and from 6.5 to 7.5 kbar in northern VT indicating an increase in peak burial of 3-6 km from north to south. Along the western end of the central VT traverse, there are differences in measured Raman shifts and inferred peak pressures of up to 1kbar across the Richardson Memorial Contact (RMC), indicating a possible fault contact with minor post-peak metamorphic shortening of up to ~3 km. In contrast, along an east-west traverse in the vicinity of the Goshen Dome, MA, there was little observed variation in Raman shifts across the contact. By contrast, QuiG barometry clearly indicates significant discontinuities in peak pressure east of the Strafford Dome in central VT. This supports the interpretation that post-peak metamorphic shortening was necessary to juxtapose upper staurolite-kyanite zone rocks next to lower garnet zone pelites. Overall, it is concluded that garnet core thermobarometry and garnet core isopleths may provide unreliable results for the P–T conditions of garnet nucleation and inferred P–T paths during garnet growth unless independently verified. The consistency of QuiG results with rim thermobarometry indicates that peak metamorphic conditions previously reported for the CVT using garnet rim thermobarometry are robust and that variation in QuiG barometry results is a valuable tool to analyze structural features within a metamorphic terrane.

Key words: quartz inclusion barometry; QuiG; P-T conditions; garnet zoning; Connecticut Valley Trough

INTRODUCTION

Recent advances in the application of Raman inclusion thermobarometry, in particular quartz inclusion in garnet (QuiG) Raman barometry, have afforded an exciting avenue for constraining pressure conditions of porphyroblast nucleation and growth (e.g. Ashley et al., 2014; Kohn, 2014; Spear et al., 2014; Castro & Spear, 2017a; Thomas & Spear, 2018; Wolfe & Spear, 2018; Bayet et al., 2019; Soret et al., 2019). A key advantage of QuiG is that it is an elastic thermobarometer, not a chemical thermobarometer, and therefore relies on the mechanical equilibrium of an inclusion-host system and is independent of governing assumptions of chemical equilibrium. As a result of this advantage, it is possible to examine whether a system was close to equilibrium when garnet nucleated and grew when paired with temperature constraints (e.g. thermobarometry, trace element thermometry, thermal modeling, carbonaceous material Raman thermometry). Several studies have utilized QuiG to place constraints on garnet nucleation conditions (e.g. Ashley et al., 2014; Castro & Spear, 2017a; Wolfe & Spear, 2018), and others have compared QuiG with equilibrium thermobarometry methods to confirm that garnet nucleated at P-T conditions that required considerable overstepping of its equilibrium isograd (Spear et al., 2014; Castro & Spear, 2017a; Spear & Wolfe, 2018; Wolfe & Spear, 2018). Recently, Viete et al. (2018) made fine-scale comparisons of quartz inclusion Raman shifts with rhythmic garnet compositional zoning in subduction zones to infer that cyclic pressure fluctuations occurred during the growth of garnet porphyroblasts. Spear & Wolfe (2018) observed a lack of systematic variation of Raman shifts with respect to radial position in garnet from metapelites from the Connecticut Valley Trough leading to the interpretation that garnet nucleated and grew at nearly isobaric-isothermal pressure-temperature (P-T) conditions. Both Viete et al. (2018) and Spear & Wolfe (2018, 2019) demonstrated that variations, or lack thereof, of quartz inclusion Raman shifts with respect to their radial position in garnet have significant petrological implications.

This contribution presents a comparative analysis of QuiG barometry with thermobarometry and mineral assemblage diagram analysis at three locations alongstrike of the CVT and regional trends of quartz inclusion Raman shifts throughout the terrane. The first goals

were to determine how QuiG barometry compares with equilibrium thermodynamic methods and to better constrain the P-T conditions experienced during the Acadian Orogeny (Doll et al., 1961; Thompson & Norton, 1968; Zen et al., 1983; Robinson et al., 1998) over a broad regional extent. The equilibrium thermodynamic methods considered here are conventional (exchange and net transfer) thermobarometry and the intersection of garnet core isopleths from mineral assemblage diagrams. The second set of goals is to present two applications of QuiG barometry: the first is a regional analysis of the CVT to study how the depth of burial compared along-strike, and the second is an exploration of using QuiG to map and quantify possible offset across faults and shear zones within the CVT. To accomplish these goals, we present petrological characterization of garnet-bearing rocks from the CVT and underlying Rowe-Hawley Zone, including phase identification, textural analysis, mineral compositions, garnet core-to-rim quartz inclusion Raman shift measurements, QuiG barometry, and conventional thermobarometry. The goal of the regional analysis of Raman shifts is to assess how they vary with changes in metamorphic grade and across major structural features such as the Richardson Memorial Contact (RMC). The results and interpretations presented here are the culmination of a large regional study that produced several focused studies (Spear et al., 2014; Spear & Wolfe, 2018, 2019; Wolfe & Spear 2018) and the present contribution contains the complete dataset and P-T interpretations. Particular focus is placed on describing new samples from the Goshen field area in western MA, as several central VT samples were discussed in detail by Spear et al. (2014) and Wolfe & Spear (2018).

GEOLOGICAL SETTING

The Connecticut Valley Synclinorium (CVS), or Connecticut Valley Trough (CVT), is a well-studied metasedimentary trough within the northeastern part of North America that experienced Barrovian-style metamorphism during the Acadian–Neo-Acadian Orogeny (e.g. White & Jahns, 1950; Doll et al., 1961; Zen et al., 1983; Hames et al., 1991; Robinson et al., 1998). The CVT lies above a sequence of Cambro-Ordovician rocks of the Taconic Rowe–Hawley Zone that were variably overprinted during Acadian–Neo-Acadian metamorphism (Hatch, 1969; Zen et al., 1983; Stanley & Hatch,

1988; Hames *et al.*, 1991; Cheney & Brady, 1992; Robinson *et al.*, 1998; Ratcliffe *et al.*, 2011). Armstrong *et al.* (1992) characterized the Acadian overprint of Cambro-Ordovician Taconic rocks as having reached *P-T* conditions of 4–6 kbar and 400–600 °C, whereas the CVT experienced conditions of 600–725 °C and 6-5–10 kbar. Generally, peak metamorphism occurred between ~390 and 370 Ma (Doll *et al.*, 1961; Naylor, 1971; Zen *et al.*, 1983; Vance & Holland, 1993; Robinson *et al.*, 1998; Cheney *et al.*, 2006; Aleinikoff *et al.*, 2011; Ratcliffe *et al.*, 2011; Gatewood *et al.*, 2015; Peterman *et al.*, 2016; see Supplementary Data Table S1; supplementary data are available for downloading at http://www.petrology.oxfordjournals.org).

Figure 1 shows a map of western New England with the CVT colored in purple [following the regional boundaries as presented by Robinson & Kapo (2003)] and is labeled with selected *P-T* constraints and their associated publications (for additional regional *P-T* constraints see Hames *et al.*, 1989, 1991; Cheney & Brady, 1992; Menard & Spear, 1994; Armstrong & Tracy, 2000;

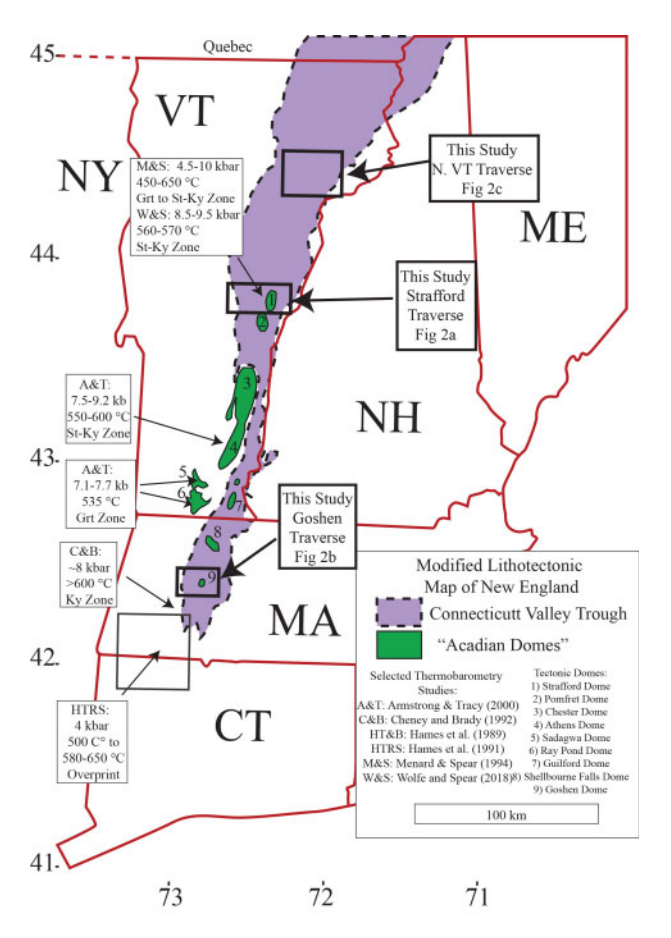


Fig. 1. Geographical map of New England with the lithotectonic extent of the CVT modified after Robinson & Kapo (2003) and Hibbard et al. (2006). The mapped extent of the CVT is colored in purple, and the tectonic domes are shown in green and numbered for orientation. Selected *P-T* conditions and locations of their studies are shown on the map with the abbreviations defined in the legend in the bottom right corner. The locations of each field site that are shown in Fig. 2 are outlined with black boxes and large bold arrows.

Spear et al., 2002). The three field areas presented in this study are outlined with bold boxes. The first field area is an east–west traverse west of the Goshen Dome in western Massachusetts, and the second central VT east–west traverse crosses the Strafford Dome in east-ern Vermont. The third field area in northern VT is a partial traverse across the same belt and includes large segments of biotite or lower grades across-strike. Geological maps of each field area are presented in Fig. 2 along with major lithologies, metamorphic isograds, sample locations, and maximum Raman shifts measured at each sample locality.

In the western Massachusetts section of the CVT (Fig. 2), the Goshen Formation is the primary Devonian metapelitic unit and is overlain by the Waits River and Gile Mountain Formations further to the east (Zen et al., 1983; Hatch & Stanley, 1988). Hatch (1969), Hatch & Warren (1981) and Hatch & Stanley (1988) mapped the Goshen Formation as continuous with the Northfield Formation in Vermont (Doll et al., 1961), and the Gile Mountain and Waits River Formations are the dominant formations in eastern and northern Vermont (Doll et al., 1961; Ratcliffe et al., 2011).

ANALYTICAL METHODS

Raman spectroscopy of quartz inclusions was performed on both standard thin (30 μm) and thick (60 μm) polished sections of metapelitic and metavolcanic samples for QuiG barometry (Kohn, 2014). Measurements of Raman spectra were performed on a Bruker Senterra Raman Microprobe at Rensselaer Polytechnic Institute using a 532 nm green laser and 1800 grooves per mm grating. Each measurement, unless otherwise noted, was collected at six coadditions of 10 s for a total of 60 s with a 100×, 0.9 N.A. objective. Spectral resolution of the Bruker Senterra is ~3.0 cm⁻¹, and the precision of the fitted peak positions of Raman bands using the full width half maximum (FWHM) of the 464 cm⁻¹ band are 0.1-0.2 cm⁻¹. The Bruker Senterra performs an internal calibration on a neon line before every inclusion measurement and instrument drift was monitored by periodic measurement of a Herkimer quartz polished mount.

QuiG barometry utilizes the pressure sensitivity of the 464 cm⁻¹ Raman band (Hemley, 1987) to constrain the pressure conditions where garnet overgrew a quartz inclusion. The calibration of Schmidt & Ziemann (2000) was used to calculate the internal pressure currently experienced by encapsulated quartz inclusions from the positive or negative shift of a quartz inclusion's 464 cm⁻ ¹ Raman band relative to an unconstrained reference quartz grain. The reference quartz is either unstrained matrix quartz or large quartz inclusions in garnet that have been fully exposed. Entrapment conditions are constrained by projecting a curve of constant volume, or isomeke (Rosenfeld, 1969), between quartz and garnet in P-T space using the elastic model of Guiraud & Powell (2006) with the Angel et al. (2017) updates, and the piston cylinder empirical calibration of Thomas &

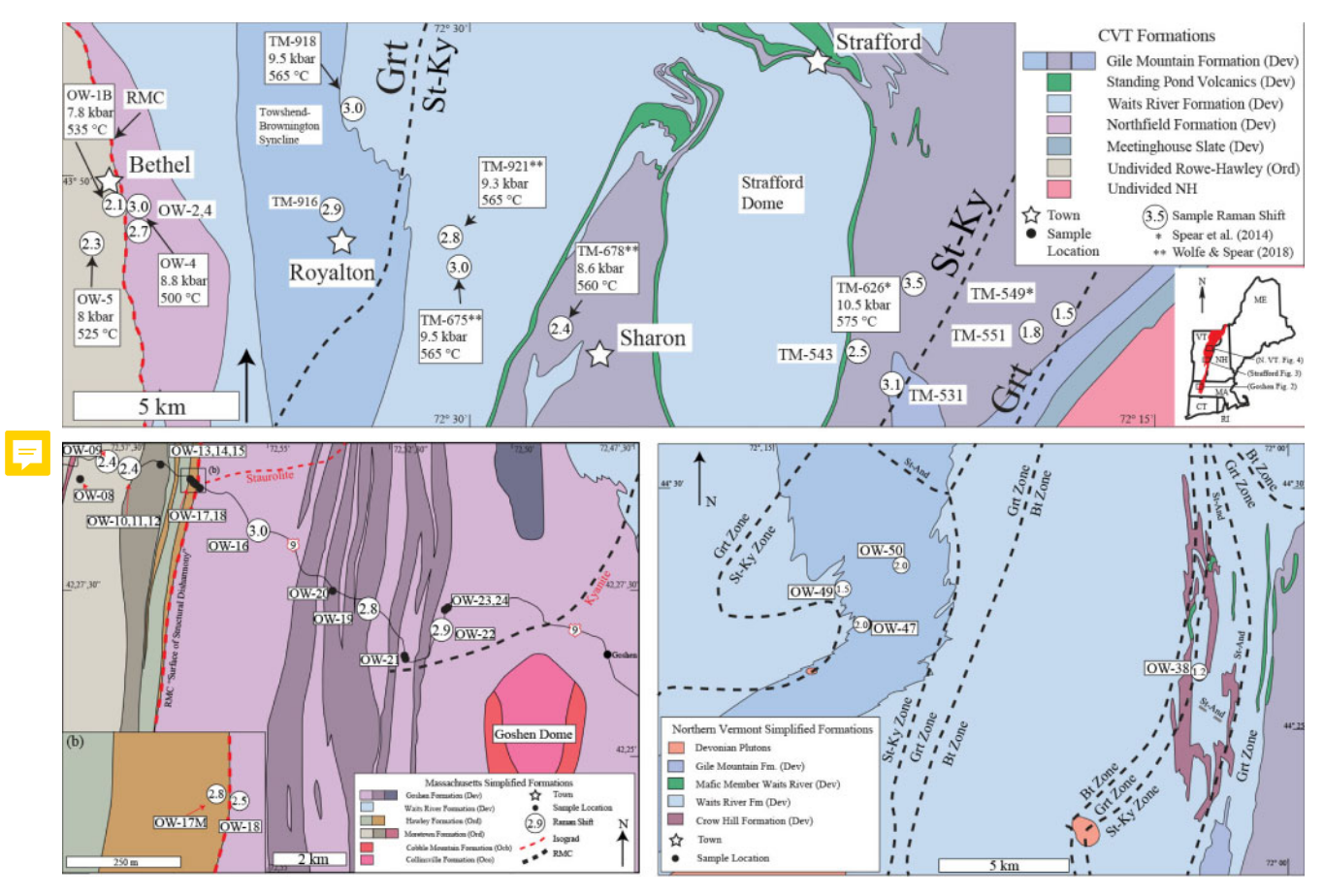


Fig. 2. (a) Geological map of the CVT for the central VT traverse modified after Ratcliffe *et al.* (2011), showing the locations of samples with Raman shift data and *P*–*T* results. The circled number in each sample location shows the maximum Raman shift for that sample. *P*–*T* conditions are also noted where available in the sample label. Samples with (*) denote Raman shifts and/or *P*–*T* data from Spear *et al.* (2014) and (**) denotes *P*–*T* results from Wolfe & Spear (2018). (b) Geological map of western Massachusetts near the Goshen dome modified after Hatch (1969) and Hatch & Warren (1981), showing sample locations and respective Raman shifts. Inset geological map in (c) shows the locations of samples collected across the RMC within the Hawley Fm. (d) Geological map of the CVT of the northern VT traverse modified after Doll *et al.* (1961) and Ratcliffe *et al.* (2011), showing the locations of samples with their maximum Raman shifts (numbers in open circles).

Spear (2018). Uncertainty of QuiG barometry isomekes measurements are of the order of ± 0.5 kbar (Thomas & Spear, 2018; Wolfe & Spear 2018).

Mineral compositions were determined on the Cameca SX-100 electron microprobe at Rensselaer Polytechnic Institute. Silicate mineral analyses were collected using a 20 nA beam with a 1 µm spot size for silicates, and 5 µm spot size for sheet silicates. Microprobe analyses were calibrated with both synthetic and natural standards. X-ray maps of samples were also collected using the Cameca SX-100 at Rensselaer Polytechnic Institute with both wavelengthdispersive and energy-dispersive spectrometers. Maps were not corrected for background, and were collected over a variety of step sizes and dwell times with a 100 nA beam current. Bulk-rock compositions were collected using energy-dispersive spectrometry scans of thin sections with a 40 µm beam run over rectangular line scans with a line step of 40 µm, similar to the method used by Castro & Spear (2017) and Wolfe & Spear (2018).

Temperatures were determined using garnet-biotite (Grt-Bt), garnet-hornblende (Grt-Hb) Fe-Mg, and garnet-ilmenite (Grt-Ilm) exchange thermometry using the calibrations of Hodges & Spear (1982), Graham & Powell (1984), and Pownceby et al., (1991) respectively. Metamorphic pressures were constrained with garnetplagioclase-muscovite-biotite barometry (GPMB) using the calibration of Hodges & Crowley (1985). Mineral assemblage diagrams (MADs) were prepared in the MnNCKFMASH system using the Fortran program Gibbs (Spear & Menard, 1989), with the SPaC 2014 thermodynamic dataset (Spear & Pyle, 2010). The SPaC dataset is modified from the thermodynamic dataset of Berman (1988), and thermodynamic data and solution models are fully described in the appendix of Spear & Pyle (2010). Briefly, solution models in the SPaC dataset are ideal ionic solution models, with the exception of the garnet non-ideal solution model from Berman (1990). Muscovite, biotite, and chlorite are calculated with multisite mixing. The primary focus of this contribution is on using the common tangent method of calculating garnet core isopleths typically employed in metamorphic petrology studies (e.g. Tinkham & Ghent, 2005). The parallel tangent was not used here and readers are referred to Spear & Wolfe (2018, 2019) for a detailed exploration of parallel tangent or maximum driving force (MDF) isopleths and the effect of the effective bulk composition on their calculation (see also Hillert, 2008; Pattison & Tinkham, 2009; Pattison *et al.*, 2011; Spear *et al.*, 2014; Spear & Pattison, 2017). As MDF modeling is not the focus of this contribution, all results and discussion are focused on the application of the common tangent method.

PETROGRAPHY, GEOCHEMISTRY, AND RAMAN SHIFTS

This section contains an example of the overall approach applied to each sample using sample OW-16 from the Goshen traverse. Locations of each sample, their mineral assemblages, mapped metamorphic grade, and highest Raman shifts are reported in Tables 1 and 2. Bulk-rock chemistry for each sample is found in Supplementary Data Table S2 and chemical spot analyses for major phases are tabulated in Supplementary Data Table S3. All inclusion Raman shifts for the Goshen traverse samples can be found in Table 3. Detailed petrographic descriptions and X-ray maps for any Goshen traverse samples not included in the main text are located in Supplementary Data Figs

S1–S7. It is important to note that a subset of central VT samples were previously examined in detail by Spear et al. (2014; TM-549 and TM-626) and Wolfe & Spear (2018; TM-921, TM-678, TM-675), and readers are referred to those papers for petrography and P–T discussion. All other central VT and northern VT samples are discussed in Supplementary Data Figs S8–S19. Raman data for all Vermont samples from Spear & Wolfe (2018) and Wolfe & Spear (2018) are summarized in Supplementary Data Tables S4. All mineral and endmember abbreviations follow Kretz (1983).

In each sample, the largest garnet was selected to examine for QuiG barometry. In several cases (e.g. OW-16) center cuts could be verified by examining crystallographically oriented inclusion traces in garnet. In other samples, the largest garnet was examined as a closest to center cut as possible. The main criteria for selecting quartz inclusions for QuiG barometry were to find grains that were uncrowded [at least three times the radius in garnet around the inclusion, following Kohn (2014)], not cracked, and not near a surface or fracture in garnet. Cracked and exposed grains were avoided, except to determine the baseline for unpressurized quartz in the case of large inclusions, and additional grains were measured when crowding occurred. Inclusions that are variably crowded were observed to have a significant Raman shift although typically less than uncrowded inclusions. Radial positions of quartz inclusions were approximated by the inclusion's radial

Table 1: Sample locations, mineral suites and maximum Raman shifts

Sample	Latitude	Longitude	Formation name	Terrane age	Field area
OW-9	42.49089	<i>–</i> 72⋅97067	Moretown	RH	Goshen
OW-11B	42.48931	–72·96199	Moretown	RH	Goshen
OW-17M	42.48549	<i>–</i> 72·94014	Hawley	RH	Goshen
OW-18	42.48517	-72 ⋅93960	Goshen	CVT	Goshen
OW-16	42.47344	–72·91905	Goshen	CVT	Goshen
OW-19 [*]	42.45414	–72·88191	Goshen	CVT	Goshen
OW-22	42.44863	-72 ⋅85645	Goshen	CVT	Goshen
OW5C*	43.82549	-72-62492	Moretown	RH	Bethel
OW1B	43.82581	-72-62794	Barnard Gneiss	RH	Bethel
OW-2	43.82561	-72-62250	Northfield	CVT	Bethel
OW4	43.81273	-72 ⋅64828	Northfield	CVT	Bethel
TM-916C	43.82365	−72 ·54980	Gile Mountain	CVT	Strafford
TM-918C*	43.85022	−72 ·54277	Gile Mountain	CVT	Strafford
TM-921*†	43.81378	−72 ·50553	Waits River	CVT	Strafford
TM-675*†	43.80940	<i>–</i> 72⋅50371	Waits River	CVT	Strafford
TM-678*†	43.79084	-72 ⋅46447	Gile Mountain	CVT	Strafford
TM-531	43.78078	-72 ⋅34358	Gile Mountain	CVT	Strafford
TM-543	43.78847	-72 ⋅35206	Gile Mountain	CVT	Strafford
TM-626*‡	43.80450	-72 ⋅33500	Gile Mountain	CVT	Strafford
TM-551	43.79022	-72 ·29461	Gile Mountain	CVT	Strafford
TM-623	43.79114	<i>–</i> 72⋅31525	Gile Mountain	CVT	Strafford
TM-549*‡	43.79511	-72 ⋅28250	Gile Mountain	CVT	Strafford
OW-47	44.45386	−72 ·20595	Gile Mountain	CVT	Northern VT
OW-49	44.46581	-72 ·21758	Gile Mountain	CVT	Northern VT
OW-50	44.47538	-72·18924	Gile Mountain	CVT	Northern VT
OW-38	44.43648	-72.04450	Waits River	CVT	Northern VT

^{*}Spear et al. (2014) sample data.

tWolfe & Spear (2018) sample data.

[‡]Spear & Wolfe (2018) sample data.

RH,

^{**}Rowe-Hawley; CVT, Connecticut Valley Trough.

Table 2: Mineral suites and maximum Raman shifts

Sample	Rock type	Grade	Assemblage	Garnet inclusion suite	Shift (464 ^{–1} cm)
OW-9	Metapelite	Grt zone	Qtz-Pl-Ms-Chl-Bt-Grt-Mag-Ep-Ap-Zrc-Ilm	Qtz-Ep-Ap-Zr-IIm-Mag	2.4
OW-11B	Metapelite	Grt zone	Qtz-Pl-Ms-Chl-Bt-Grt-Ilm	Qtz-Ap-IIm	2.4
OW-17M1	'Pinstripe Granofels'	Grt zone	Chl-Grt-Bt-Ap-Ilm-Qtz-Pl-Ms-Zrc-Ep	Qtz-IIm-Ep-Ap-Zrc	2.8
OW-18	Metapelite	St zone	Qtz-Ms-PI-Bt-Grt-IIm-Rt-ChI-Ap-Zrc-Gr-Tur	Qtz-Ilm-Ap	2.5
OW-16	Metapelite	St zone	Otz-Ms-PI-Bt-Grt-St-IIm-Rt-ChI-Ap-Zrc-Gr- Mnz	Qtz–IIm	3.0
OW-19	Metapelite	St zone	Qtz-Ms-Pl-Bt-Grt-Ilm-Chl-Ap-Zrc-Gr-Mnz	Qtz-Rt-IIm-Ap	2.8
OW-22	Metapelite	St–Ky zone	Otz-Ms-Pl-Bt-Grt-St-IIm-Chl-Ap-Zrc-Gr-Mnz- Tur	Qtz-Ap-Zrc	2.9
OW5C*	'Pinstripe Granofels'	Grt zone	Otz-Ms-Pl-Bt-Grt-Ilm-Chl-Py-Ap-Zir-Tur-Ep	Qtz-PI-Ep-Tur-Ap-IIm	2.3
OW1B	Metavolcanic	Grt zone	Qtz-Hbld-Pl-Chl-Grt-Ap-Ep-Ilm-Hem	IIm-Ap-Ep-Qtz-Hem	2⋅1
OW-2	Metapelite	Grt zone	Otz-Ms-Pl-Chl-Grt-Gr-Ap-llm	Qtz-Ap-IIm-Gr	2.9
OW4	Metapelite	Grt zone	Qtz-Ms-Pl-Bt-Chl-Grt-Gr-Ap-Ilm	Qtz-Gr-Ap-IIm	2.7
TM-916C	Metapelite	Grt zone	Otz-Ms-PI-Bt-Grt-Ilm-ChI-Ep-Aln-Py-Ap-Cal- Tur-Gr	Qtz-Ap-IIm-Py	2.9
TM-918C*	Metapelite	Grt zone	Otz-Ms-PI-Bt-Grt-IIm-ChI-Py-Ap-Zrc-Tur-Gr- Rt	Qtz-Ap-IIm-Py-Zr	3.1
TM-921*†	Metapelite	St–Ky zone	Otz-Ms-PI-Bt-Grt-Ep-St-Aln-Chl-Rt-Ilm-Py- Po-Ap-Xen-Zrc-Gr	Qtz-Rt-IIm-Ep-AIn-Py- Ap-Zrc	2.8
TM-675*†	Metapelite	St-Ky zone	Otz-Ms-PI-Bt-Grt-Ep-Ilm-ChI-Rt-Ap-Zrc- Mnz-Tur-Gr	Qtz-Ap-Rt	3.0
TM-678*†	Metapelite	St–Ky zone	Otz-Ms-PI-Bt-Grt-IIm-ChI-Rt-Ap-Zrc-Tur-Ep- Gr	Otz-Ms-Bt-Pl-Ep-Rt-IIm	2.4
TM-531	Metapelite	St-Ky zone	Qtz-Grt-Ms-PI-Bt-Ky-IIm-Ap-Zrc	Qtz-Zrc-Ap	3.1
TM-543	Metapelite	St–Ky zone	Qtz-Grt-Ms-PI-Bt-Rt-IIm-Ap-Zrc	Qtz .	2.6
TM-626*‡	Metapelite	St–Ky zone	Qtz-Ms-Pl-Bt-Grt-St-Chl-Rt-Ilm-Tur	Qtz–Rt	3.5
TM-551	Metapelite	Grt zone	Qtz-Pl-Grt-Ms-Bt-Chl-IIm	Qtz	1.8
TM-623	Metapelite	Grt zone	Qtz-Grt-Ms-PI-Bt-IIm-Ap-Zrc	Qtz	1.5
TM-549*‡	Metapelite	Grt zone	Qtz-Ms-PI-Bt-Chl-Grt-IIm	Qtz–Ilm	1⋅5
OW-47	Metapelite	St–Ky zone	Qtz-Ms-PI-Bt-Grt-St-IIm-Gr-Zrc	Qtz Ap	1.9
OW-49	Metapelite	St–Ky zone	Qtz-Ms-PI-Bt-Grt-St-IIm-Gr-Zrc	Qtz	1.5
OW-50	Metapelite	St–Ky zone	Qtz-Ms-Pl-Bt-Grt-St-Ilm-Chl-Ap-Mnz-Gr	Qtz-Ap-IIm	2
OW-38	Metapelite	St–And zone	Qtz-Ms-Pl-Bt-Grt-St-Ilm-Chl-Ap-Mnz-Gr-Ep	Qtz-Ap-Mnz-Gr	1⋅2

^{*}Spear & Wolfe (2018) sample data.

distance from the center relative to the radius and normalized to a scale of 0–1.

Petrography of OW-16

OW-16 is a staurolite zone metapelite collected west of the RMC from the Goshen Formation and the full thin section scan and photomicrograph of a garnet porphyroblast are shown in Fig. 3. The assemblage is typical for this grade with prograde garnet, biotite, and staurolite porphyro- or poikiloblasts overgrowing a matrix of Ms-Qtz-Pl-Gr-Ilm-Chl. Minor phases are apatite, zircon, relict monazite, and pyrite. Chlorite occurs only as retrograde replacement of biotite and as late matrix grains that cut across the matrix foliation. Garnet porphyroblasts typically range from 2 to 3 mm in diameter and have radiating traces of quartz inclusions that were the target for QuiG barometry (see Raman shift labels in Fig. 3b). These inclusion traces terminate at about \sim 70–80% of the radial distance to the rim where they intersect a cloudy inclusion texture coincident with the crystal face that is composed of graphite, apatite and sparse quartz inclusions. The maximum Raman shift preserved in the garnet core is 3.0 cm⁻¹. Notably, there is almost no core-to-rim variation in Raman shifts as shifts up to $2.8 \, \text{cm}^{-1}$ are found in the outer rim area beyond the cloudy graphite texture where the trace of aligned quartz inclusions terminated.

Figure 4 shows that garnet zoning is concentric and typical for a metapelitic garnet growth zoning (Hollister, 1969) except X_{grs} . The X-ray map in Fig. 4b shows garnet to be weakly zoned in X_{grs} with a low concentration in the core and on the rim and with slight enrichment between them. Of note is the diffuse band of enrichment in $X_{\rm sps}$ in the outer mantle of the garnet (Fig. 4a). This band is roughly coincident with the band of graphite inclusions. The zone of low X_{grs} and $X_{\rm Fe}$ at the rim is also coincident with the outermost graphite-rich zone. Plagioclase cores range in composition from An₂₂ to An₂₆ whereas rims decrease in composition to An₁₄ with a fringe of An₅₋₇ (Figs 4b and 5). Biotite compositions range from X_{Fe} contents $[X_{Fe} = Fe/(Fe + Mg)]$ of 0.422 to 0.460 and show little zoning.

tWolfe & Spear (2018) sample data.

[‡]Spear et al. (2014) sample data.

Table 3: Summary of Raman shifts for quartz inclusions

Sample	Mineral	Ref. peak position (cm ⁻¹)	Av. peak (cm ⁻¹)	Inc. shift (cm ⁻¹)	Radial position
OW-11B	Inc3	465-22	466-97	2.03	0.37
OW-11B	Inc5	465-22	467 ⋅ 65	2.43	0.39
OW-11B	Inc7	465-22	466-92	1.70	0⋅24
OW-11B	Inc8	465-22	467.15	1.94	0.18
OW-11B	Inc10	465·22	467·50	2.28	0.10
OW-11B OW-11B	Inc12	465·22	466-65	1.43	0.43
OW-11B OW-11B	Inc13 Inc14	465·22 465·22	465⋅53 466⋅01	0⋅32 0⋅80	0·50 0·57
OW-11B OW-11B	Inc15	465.22	465·77	0.55	0.43
OW-11B	Inc16	465.22	467·61	2.39	0.39
OW-11B	Inc17	465.22	467.30	2.08	0.39
OW-11B	Inc17b	465.22	467.01	1.80	0.39
OW-11B	Inc18	465-22	466-45	1.23	0.63
OW-16	Inc1 apatite	_	964-29	_	0.59
OW-16	Inc2	465.33	468-31	2.97	0.22
OW-16	Inc4	465⋅36	466-82	1.46	0.27
OW-16	Inc5	465-36	467.30	1.94	0⋅27
OW-16	Inc6	465.36	465.76	0.39	0.26
OW-16	Inc7	465.36	467.70	2.34	0.19
OW-16	Inc8	465.36	467.40	2.04	0.19
OW-16	Inc9	465·36	467-20	1.84	0.26
OW-16	Inc10	465-36	468·09	2.73	0·37
OW-16 OW-16	Inc11 apatite	_	964.76	<u> </u>	0⋅78 0⋅87
OW-16 OW-16	Inc12 apatite Inc13	 465·36	965·46 465·40	<u> </u>	
OW-16	Inc13b	465.24	466.43	1.20	_
OW-16	Inc14	465.24	468-07	2.83	0.67
OW-16	Inc15 apatite		965.04	_	0·72
OW-16	Inc16 apatite	_	964.58	_	0.82
OW-16	Inc17	465-24	468.02	2.79	0.76
OW-16	Inc18	465.24	467.70	2.46	0.42
OW-16	Inc18 (surface)	465.24	465-33	0.09	_
OW-16	Inc1 in St	465-04	466-39	1.35	_
OW-16	Apatite	_	965.14	_	_
OW-16	Inc19	465.04	467.92	2.88	0⋅25
OW-16	Inc 20	465.04	467-69	2.65	0.29
OW-16	Inc22	465·10	467-64	2.54	0.17
OW-16	Inc23	465·10	467·96	2.86	0.11
OW-16 OW-16	Inc24 Inc25	465·10 465·10	468·07 467·62	2⋅97 2⋅51	0·09 0·09
OW-16 OW-17M	Inc11	465.04	467·84	2·80	0.40
OW-17M	Inc12	465.04	467.30	2.26	0.51
OW-17M	Inc13 zircon	-	1010.19	_	0.92
OW-17M	Inc15 zircon	_	1012⋅55	_	1.00
OW-17M	Inc 16 apatite	_	964-87		0.98
OW-17M	Inc17 apatite	_	964-81	_	0.73
OW-17M	Inc19	464.72	464-66	-0.06	0.48
OW-17M	Inc20	464.72	465·94	1.22	0.53
OW-17M	Inc21	464.72	466.40	1.68	0.44
OW-17M	Inc22 zircon	464.72	1012-11	 0.75	0.36
OW-17M	Inc23	464.72	467.48	2.75	0.31
OW-17M	Inc24	464·72	467·40	2.68	0.28
OW-17M OW-18	Inc25	464·72 464·66	467·14 467·15	2·42 2·49	0.25
OW-18	Inc1 Inc2	464.66	464·96	2.49	_
OW-18	Inctest1	464-66	466-25	_	_
OW-18	Inc1	464-82	466-87	2.04	0.80
OW-18	Inc2	464.82	466.70	1.88	0.65
OW-18	Inc3	464-82	467.02	2.20	0.55
OW-18	Inc4	464.82	465.78	0.96	0.58
OW-18	Inc5	464-82	466-45	1.63	0.62
OW-18	Inc6	464-82	466-22	1.40	0.72
OW-19	Inc1	465·15	467.96	2.81	0.07
OW-19	Inc2	465.15	466-46	1⋅31	0.20
OW-19	Inc3	465·15	467.70	2.56	0.29
OW-16	Inc26	465-10	468-03	2.93	0.08
OW-17M	Inc1	465.04	466.52	1.48	0.69
OW-17M	Inc2	465.04	466.70	1.65	0.67
OW-17M	Inc3	465·04	467·51	2.47	0.66
OW-17M	Inc3 redo	465-04	467⋅31	2⋅27	0.37

(continued)

Table 3: Continued

Sample	Mineral	Ref. peak position (cm ⁻¹)	Av. peak (cm ⁻¹)	Inc. shift (cm ⁻¹)	Radial position
OW-17M	Inc4	465-04	466.88	1.84	_
OW-17M	Inc5	465-04	466-52	1.48	0.37
OW-17M	Inc6	465.04	465.95	0.91	0.31
OW-17M	Inc7	465.04	466-84	1.80	0.27
OW-17M	Inc8	465.04	467·19	2⋅15	0.36
OW-17M	Inc9	465.04	467.03	1.98	0.40
OW-17M	Inc10	465.04	467.03	1.98	0.40
OW-19	Inc4	465.15	466-25	1.10	0.34
OW-19	Inc5	465.15	465.59	0.45	0.36
OW-19	Inc6	465.15	467·10	1.95	0.50
OW-19	Inc7	465.15	467.71	2.56	0.65
OW-19	Inc8	465.15	467.33	2⋅18	0.65
OW-19	Inc9	464-87	467.57	2.42	0.78
OW-19	Inc10	_	965-01	_	0.96
OW-19	Inc11	464-87	466.72	1.85	0.96
OW-22A	Grt1 Lrg Inc	464-76	464.76	0.00	_
OW-22A	Inc1	464.76	463.98	-0.79	_
OW-22A	Inc2	464.76	467-22	2.46	_
OW-22A	Inc3	464.76	462-81	−1 .95	_
OW-22A	Inc3 redo	464.76	462-91	–1 ⋅85	_
OW-22A	Inc4	464.76	466-32	1.56	_
OW-22A	Inc5	464.76	464-37	-0.39	_
OW-22A	Lrg Inc	464-81	464-81	0.00	_
OW-22A	Inc6	464-81	467-69	2.88	_
OW-22A	Inc7	464-81	465-49	0.68	_
OW-22A	Inc8	464-81	463.45	−1 ·36	_
OW-22A	Inc9 Apatite	_	963-28	0.00	_
OW-22A	Grt3 Inc2	464-81	464-44	-0⋅37	_
OW-22A	Grt3 Inc4	464-81	464-92	0.11	_
OW-22A	Grt3 Inc5	464-81	463-63	−1 ·18	_
OW-22A	Grt 3Inc7	464-81	462.41	-2 ⋅40	_
OW-22A	Grt3 Lrg Inc	464-81	465-20	0.39	_

Porphyroblast-scale Raman shift trends

Generally, garnet porphyroblasts from the CVT do not display any systematic variations of Raman shifts with respect to radial position, as is shown in Raman shift versus position plots for Goshen samples in Fig. 6 and Supplementary Data Figs S13 and S14, and in the study by Wolfe & Spear (2018). Goshen samples OW-11B and OW-17M (Fig. 6a and b) show little variation in the distribution of high Raman shifts over the regions where suitable inclusions were found, whereas Goshen samples OW-16 and OW-19 both show relatively flat maximum Raman shift values from core to rim as indicated by the occurrence of similarly high shift values across the traverse. In cases where multiple different shifts occur at a given radial distance, the highest shift is assumed to reflect the garnet growth conditions owing to all the factors that can lower the Raman shift (microcracking, host fractures, crowding) but no known process to increase the shift. Notably, OW-16 preserves inclusions with similar high shifts across the cloudy graphite-rich zone, suggesting that garnet growth occurred entirely on a single isomeke. Samples from the central VT traverse typically do not show core-torim variation as well (see OW-4 and TM-543 in the Supplementary Data and Wolfe & Spear 2018). The primary outliers to this generalization are observed in samples OW-22A (Goshen) and TM-678 (central VT) where a significant decrease in the Raman shift is associated with a cloudy alteration texture caused by dissolution-reprecipitation reactions (Dempster et al., 2017; Wolfe & Spear, 2018; Dempster et al., 2019). The garnet dissolution-reprecipitation textures occur along the rims and cracks of garnet and are associated with low grossular content and spessartine back-diffusion profiles where garnet was resorbed. These textures are believed to be caused by retrograde fluid infiltration and are not part of the initial garnet growth phase, and are explored in a separate contribution. The other exception is seen in central VT sample OW-2 (Supplementary Data Figs S10 and S15) where maximum Raman shifts vary from 2.7 within the core to 2.0 within the rim. This corresponds to a textural boundary where garnet cores appear to predate the matrix fabric, whereas rims overgrow the matrix fabric (Supplementary Data Fig. S10).

COMPARING QUIG BAROMETRY WITH THERMOBAROMETRY AND MADS

Select samples from the Goshen traverse were chosen on which to perform thermobarometry and to calculate mineral assemblage diagrams (MADs), including samples OW-11B and OW-17M from the Rowe–Hawley side of the RMC and samples OW-18, OW-16 and OW-19 from the Goshen Formation east of the RMC. For each sample, phase assemblages, garnet core compositional isopleths, QuiG isomekes, and rim thermobarometry results are plotted on *P-T* diagrams (Fig. 7). The vertical

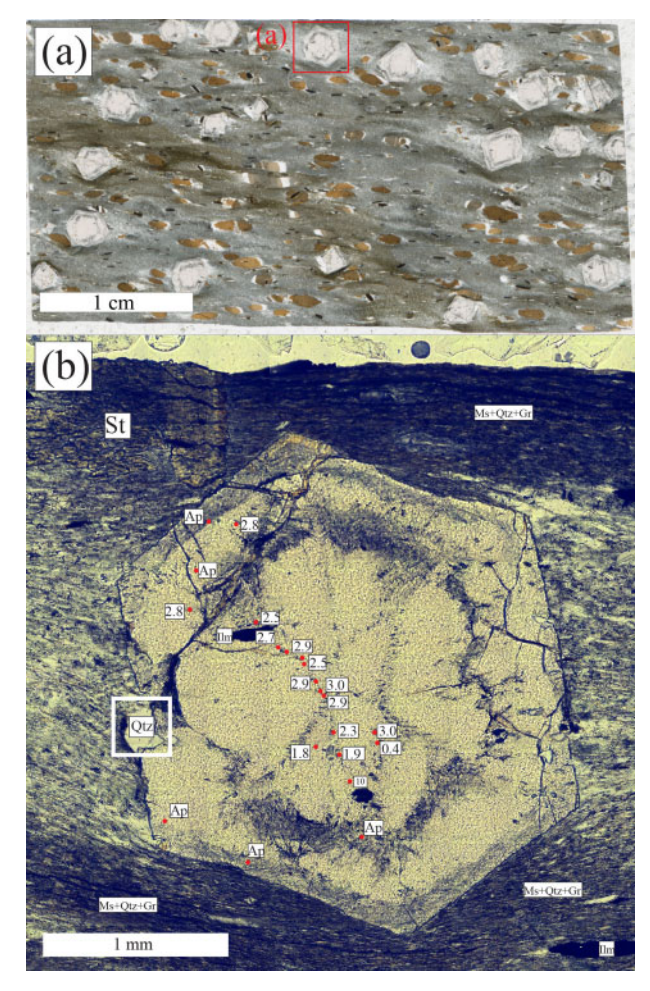


Fig. 3. (a) Full thin section scan of Goshen Fm. sample OW-16 with the location of the photomicrograph (b) outlined with the red box. (b) Photomicrograph of a garnet porphyroblast with quartz inclusions and their Raman shifts marked and labeled. Most porphyroblasts in this sample, like the one shown, have radiating core-to-rim quartz inclusion traces that end at the concentric dark graphite band midway to the rim. Quartz inclusions were measured on both sides of the graphite band. Mineral abbreviations follow Kretz (1983) for all figures.

black lines show the range of Grt-Bt KD lines that were calculated with the highest Grt Fe/(Fe + Mg) + lowest Bt Fe/(Fe + Mg) pair and lowest Grt Fe/(Fe + Mg) + highest Bt Fe/(Fe + Mg) to display the range of possible temperatures without making any assumptions about which pairs were in equilibrium. The GPMB barometry KEQ lines are labeled with the garnet and plagioclase compositions used. There was no evidence in this suite of rocks that epidote was present, except OW-17M, indicating that plagioclase was probably the primary Cabearing phase to participate in garnet-forming reactions. It was assumed that as garnet was growing it would consume calcic plagioclase, causing the matrix plagioclase to become more albitic. Therefore, when selecting garnet-plagioclase pairing for barometry, garnet cores were paired with high-An plagioclase whereas garnet rims were paired with low-An plagioclase. Typical uncertainties are of the order of ±25°C for GrtBt thermometry, and $\pm 1.0\,\mathrm{kbar}$ for GPMB barometry (Hodges & Spear 1982; Hodges & Crowley, 1985). Uncertainties on the intersection of garnet core isopleths have been estimated by Palin *et al.* (2016) to be of the order of $\pm 50\,^{\circ}\mathrm{C}$ and $\pm 1.0\,\mathrm{kbar}$, similar to those expected from thermobarometry. An additional set of MADs were prepared for sample OW-18 in Supplementary Data Fig. S19 to explore the effects of different variations on bulk-rock MnO content and garnet core composition.

MADs for Goshen samples are found in Fig. 7 and P-T results are summarized in Table 4 for the intersection of garnet core isopleths, the intersection of QuiG and Grt-Bt thermometry, and the intersection of GPMB and Grt-Bt thermometry. It is also important to note that each MAD presented in Fig. 7a-e is a partial MAD with higher grade minerals or phases left out of calculation (e.g. no MAD was calculated with melt). Several broad trends are apparent when examining the positions of QuiG isopleths, garnet core isopleths, and core-rim thermobarometry results. In each case, QuiG isomekes plotted at similar pressure conditions for the suite of samples, roughly between ~8 and 9 kbar at 550°C. Combined with the observation that Raman shifts did not typically vary with core-to-rim position within a porphyroblast, this indicates that pressures were relatively constant over the duration of garnet growth. Compared with QuiG isomekes, garnet core isopleths showed wide variability over the five samples shown. Garnet core isopleths typically plotted at some intermediate P-T conditions between the garnet-in curve and QuiG and thermobarometry results. In most cases, the garnet core isopleths plotted within 25 °C of the garnet-in curve and would typically be interpreted as garnet growth beginning at near equilibrium conditions (e.g. samples OW-16 and OW-19; Fig. 7d and e). Sample OW-11B was unique in that the garnet core isopleths plotted at substantially higher pressures than those for any other sample.

Thermobarometry results from the Goshen traverse were equally variable across the sample suite. Thermobarometry results from samples collected from the Rowe-Hawley belt to the west of the RMC (OW-11B and OW-17M; Fig. 7a and b) yield pressures for the garnet core that are higher than those for the garnet rims, which might suggest that garnet growth accompanied decompression. Thermobarometry for two other samples from the Goshen Formation (OW-16 and OW-18; Fig. 7c and d) yield core-to-rim variations that imply loading during garnet growth, an inference that is supported by comparison of the intersecting garnet isopleths with rim thermobarometry. In comparison, Goshen Formation sample OW-19 (Fig. 7e) yields P-T conditions for both garnet core and rim that are entirely consistent with garnet growth occurring isothermally and isobarically at around 560 °C, 9 kbar. However, the intersecting isopleths of garnet core compositions fall 1.0–1.5 kbar below these conditions. Figure 8 shows a summary plot comparing thermobarometry results with QuiG barometry for the Goshen traverse.

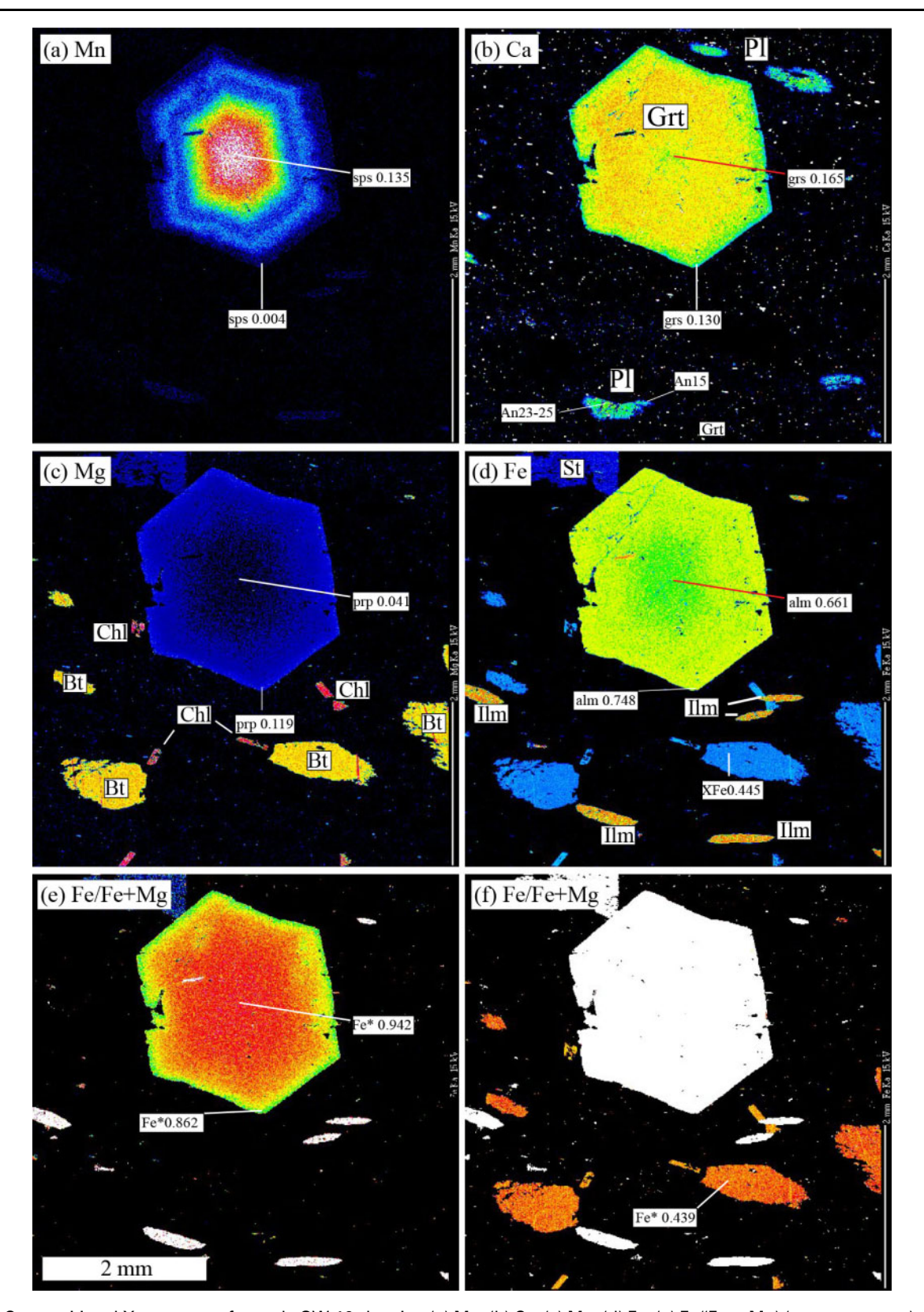


Fig. 4. Compositional X-ray maps of sample OW-16 showing (a) Mn, (b) Ca, (c) Mg, (d) Fe, (e) Fe/(Fe + Mg) (garnet contrast), and (f) Fe/(Fe + Mg) (biotite contrast). The Ca map shows that both Grt and Pl are zoned, with core-to-rim decrease in both phases.

Thermobarometry of VT traverses

New QuiG and thermobarometry results for samples near Bethel VT in the central VT traverse are

summarized in Table 5 and the results are summarized in Fig. 9, including results from Wolfe & Spear (2018). Temperatures for samples OW-5C and OW-4 were

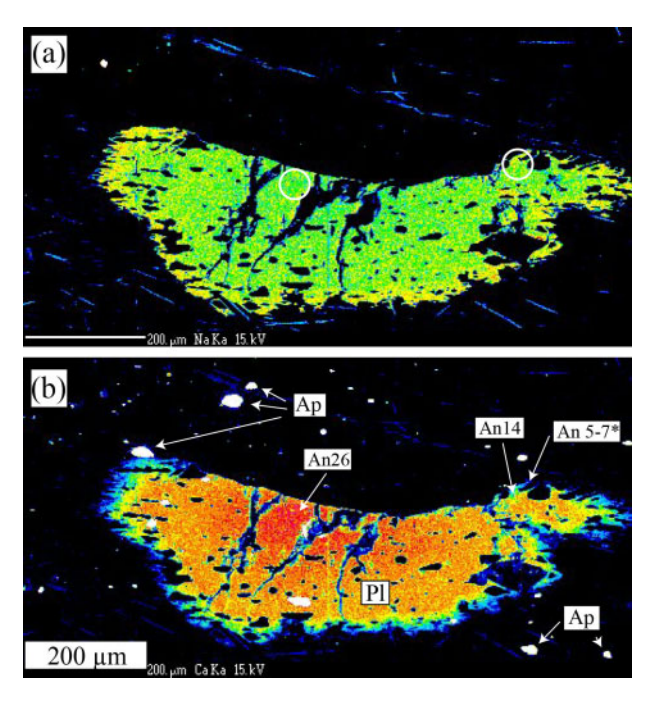


Fig. 5. Compositional X-ray maps of analyzed matrix plagioclase in sample OW-16 showing (a) Na and (b) Ca. The Ca X-ray map shows the locations of chemical analyses. The (*) denotes An contents extrapolated from the measured values.

constrained by Grt–Bt thermometry whereas Grt–Hb thermometry was used for sample OW-1B (calibration from Graham & Powell, 1984). Sample OW-5C showed nearly identical *P*–*T* conditions based on thermobarometry from the core to the rim, similar to OW-19 from the Goshen traverse (Supplementary Data Fig. S17). *P*–*T* conditions inferred from thermobarometry and QuiG from central VT are very similar to those determined from the Goshen traverse (compare Figs 8 and 9). Northern VT traverse samples typically experienced rim modification (e.g. rim replacement by plagioclase + biotite in OW-47, Supplementary Data Fig. S14d).

Figure 10 shows P-T constraints for sample OW-47 from the St-Ky zone in northern VT. Garnet porphyroblasts from this sample typically have the outer \sim 50 μ m of their rims replaced by An₁₈₋₂₀ plagioclase. This truncation of the garnet compositional rim profile coincides with an increased rim X_{Fe} that was probably not present at the original garnet rim at peak P-T conditions (Supplementary Data Fig. S14). Rim Grt-Bt thermometry was calculated by linearly extrapolating the garnet $X_{\rm Fe}$ to the original rim position (\sim 50 μ m beyond the current rim) and then pairing that projected garnet rim composition ($X_{\rm Fe} \sim 0.82$) with matrix biotite. This approach retrieved P-T conditions of ~8.5 kbar and 610 °C when paired with QuiG barometry. Alternatively, Grt-Ilm thermometry on a large ilmenite inclusion near the garnet core (calibration of Pownceby et al., 1991) with compositions of $X_{\rm sps} = 0.192$ and $X_{\rm Mn}$ in ilmenite of 0.045 yielded a temperature of \sim 555 °C at \sim 7.8 kbar along the QuiG isomeke. These two QuiG +

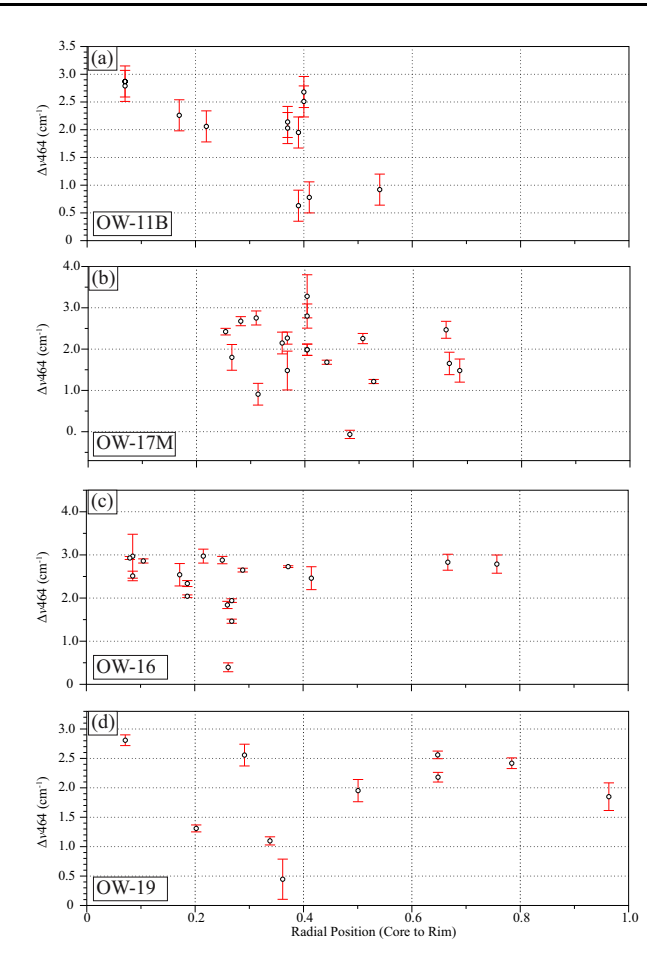


Fig. 6. Plots of Raman shifts versus normalized radial position of inclusion within garnet (core = 0, rim = 1) for samples (a) OW-11B, (b) OW-17M, (c) OW-16, and (d) OW-19. Note the lack of core to rim variation in each sample.

thermometry methods place upper and lower bounds on garnet growth respectively and the projected rim thermometry results of $\sim\!610\,^{\circ}\text{C}$ are consistent with the rock having reaching staurolite grade metamorphism. Grt–Bt thermometry (dashed lines in Fig. 10) and GPMB barometry of the current garnet rim composition retrieves lower $P\!-\!T$ conditions of $\sim\!500\!-\!550\,^{\circ}\text{C}$ and 5–6 kbar and are inferred to reflect retrograde garnet replacement after decompression, not peak metamorphism.

DISCUSSION

Based on the results of this study and data presented by Spear et al. (2014) and Wolfe & Spear (2018), the results of QuiG barometry reveal remarkable consistency both across-strike in the three traverses and along the strike of the CVT. The pressure of initial garnet growth, based on the maximum Raman shifts in the vicinity of garnet cores, varies from around 8-5 to 9-5 kbar along the Goshen and central VT traverses, and is somewhat less (6-5-7-5 kbar) in the northern Vermont traverse. Equally significant, there appears to be little to no systematic garnet core-to-rim variation in the

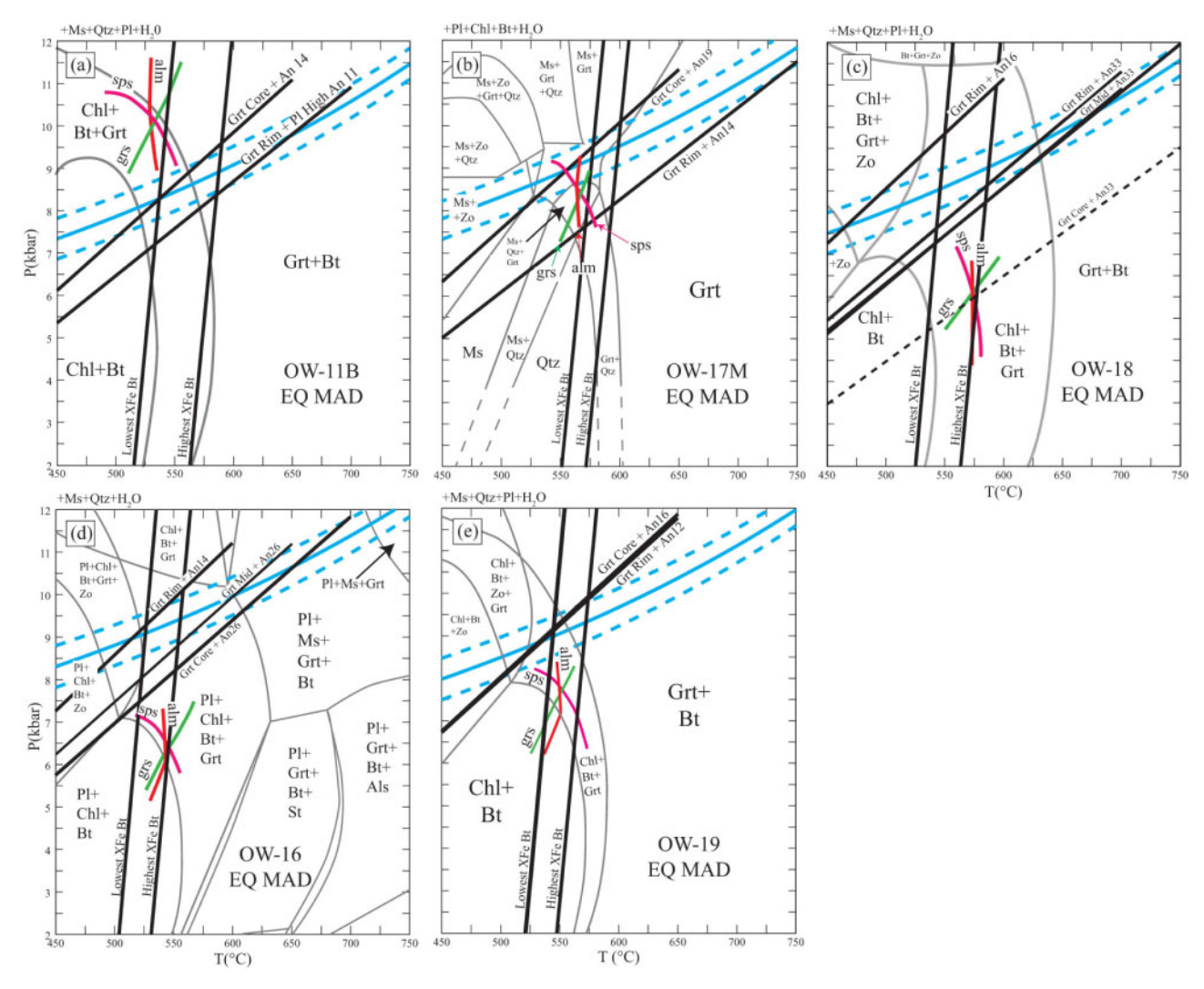


Fig. 7. *P–T* plots of the equilibrium mineral assemblage diagram (MAD) for OW-11B (a), OW-17M (b), OW-18 (c), OW-16 (d) and OW-19 (e), showing the thermobarometry results for stable mineral assemblages. Garnet core isopleths are plotted in red (alm), magenta (sps), and green (grs). QuiG isomekes are plotted as light blue curves with 0.5 kbar uncertainty envelopes. Bold black lines show rim garnet-biotite thermometry labeled for the maximum range of results [highest Fe/(Fe + Mg) Grt-lowest Fe/(Fe + Mg) Bt. GPMB barometry is shown by bold black lines labeled with the garnet-plagioclase pairing for both the garnet core and garnet rim. It should be noted in (c) and (d) that three different garnet compositions were used for GPMB barometry: core, middle, and rim. The garnet core GPMB result is shown with a dashed line as it is completely incompatible with the QuiG isomeke and is probably an indication that the garnet core was never in equilibrium with the matrix plagioclase.

Table 4: Summary of QuiG and thermobarometry results for the Goshen traverse

Sample	Core isopleths <i>P</i> (kbar)	Core isopleths T (°C)	P QuiG (kbar)	T Grt−Bt (°C)	P GPMB (kbar)	T Grt–Bt (°C)
OW-11B	~10	∼530	8·6 ± 0·5	560 ± 25	7·7 ± 1·0	560 ± 25
OW-17M	~8.5	∼560	9.4 ± 0.5	585 ± 25	7.4 ± 1.0	580 ± 25
OW-18	$\sim\!\!6$	∼575	8.8 ± 0.5	570 ± 25	9.3 ± 1.0	570 ± 25
OW-16	\sim 6·3	∼540	9.3 ± 0.5	540 ± 25	10.3 ± 1.0	545 ± 25
OW-19	~7.7	${\sim}540$	9 ± 0.5	560 ± 25	9.1 ± 1.0	560 ± 25

maximum Raman shifts (e.g. Fig. 3; see also Wolfe & Spear, 2018). The implication of this latter result is that the pressure did not change substantially over the interval in which garnet grew. Indeed, the data best support the interpretation that garnet grew at nearly isothermal, isobaric conditions at near peak conditions.

Generally, peak metamorphic conditions obtained from classical thermobarometry on garnet rims for both the Goshen and central VT traverses are consistent with results from QuiG barometry. Thermobarometry results, specifically the peak *P-T* results from garnet rim thermobarometry and QuiG, are consistent with the

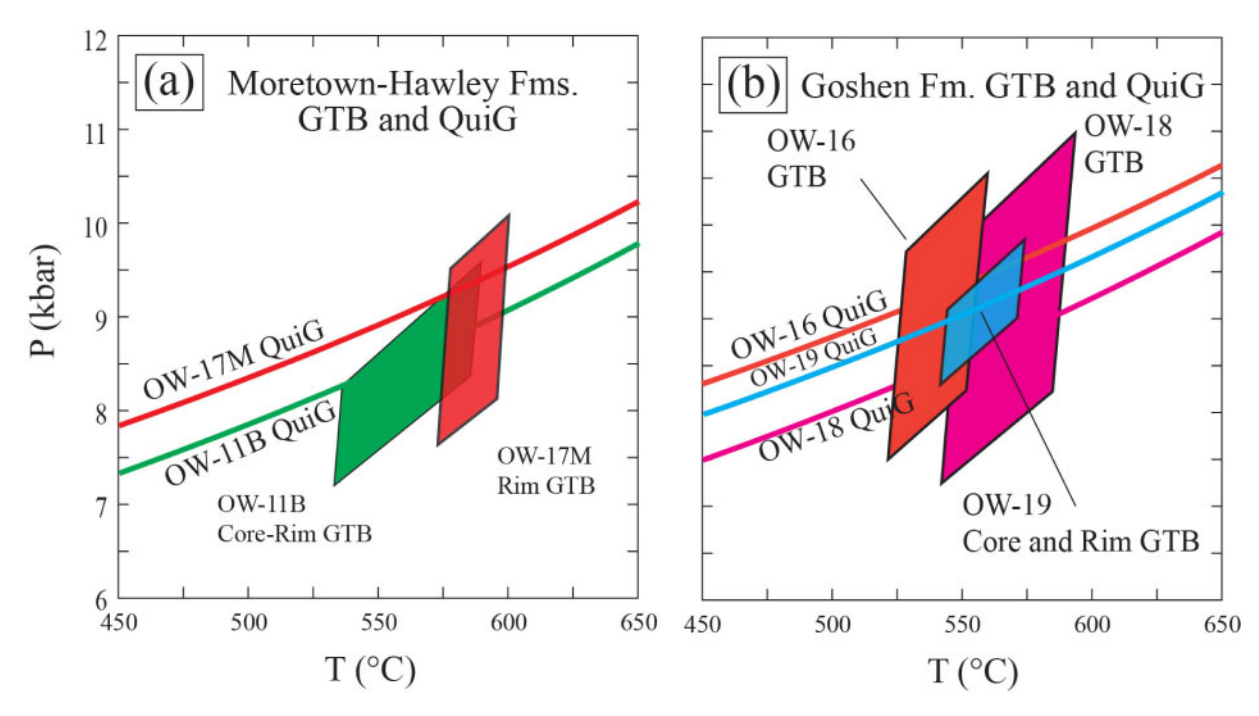


Fig. 8. P-T diagrams showing rim thermobarometry and QuiG results for samples along the Goshen traverse west of the RMC (a) and east of the RMC (b). QuiG isomekes, thermobarometry isomekes and core isopleth stars are color coded for each sample: OW-11B, green: OW-17M, red: OW-18, purple: OW-16, orange: OW-19, light blue.

Table 5: Summary of QuiG and thermobarometry results for the Stafford traverse

Sample	Pressure QuiG (kbar)	Temperature (°C)
TM-921*	9·3 ± 0·5	565 ± 15
TM-675 [*]	9.5 ± 0.5	565 ± 15
TM-678*	8.6 ± 0.5	560 ± 15
TM-918C [†]	9.5 ± 0.5	565 ± 25
OW-4	8.8 ± 0.5	500 ± 25
OW-1B	7.8 ± 0.5	535 ± 25
OW-5C [†]	8.0 ± 0.5	525 ± 25

^{*}Wolfe & Spear (2018) sample.

wealth of petrology studies performed through the CVT. South of the Goshen traverse, Hames et al. (1989) determined peak conditions of 8.2 ± 1.6 kbar and 575 ± 60 °C for the Rowe-Hawley Belt near the Waterbury Dome in western Connecticut. Subsequently, Hames et al. (1991) described progressive Acadian overprinting of Taconic metamorphic rocks starting at 500 °C, with peak overprint temperatures reaching 580-650°C in the Taconic terranes of southwestern Massachusetts. In southern Vermont, between the Goshen and central VT traverses, Armstrong & Tracy (2000) reported peak P-T conditions of 535 ± 25 °C and 7-1–7-7 kbar for garnet zone rocks in the vicinity of the Ray Pond and Sadawga Domes; and 550 ± 25 °C and 7.5-7.8 kbar for staurolite zone rocks and 600 ± 25 °C and 8.4-9.2 kbar for kyanite zone rocks near the Athens Dome. In a similar field area to this study's central VT traverse, Menard & Spear (1994) found peak conditions in the range of 500-650°C and

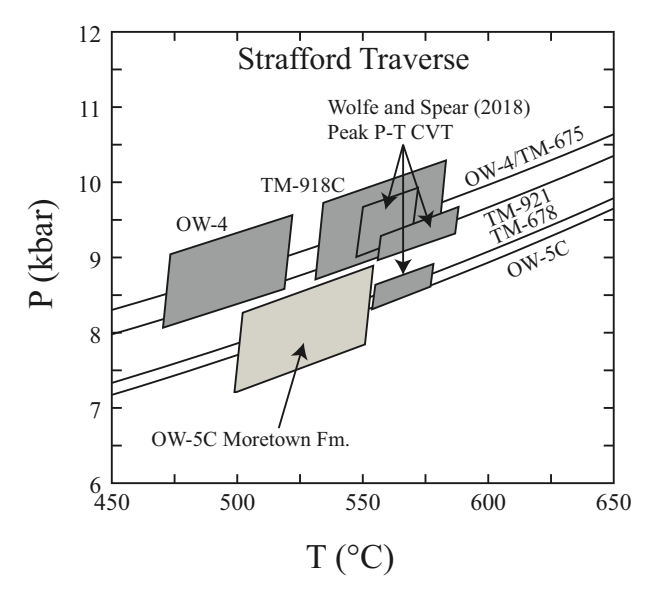


Fig. 9. *P-T* diagram showing QuiG and thermobarometry results (Grt–Bt and GPMB) from the central VT traverse, including results from Wolfe & Spear (2018). The intersection of QuiG and Grt–Bt thermometry was used for OW-5C and OW-4, whereas Grt–Hb thermometry was used for OW-1B (calibration from Graham & Powell, 1984). The dark boxes indicate *P-T* results from the CVT samples (Northfield, Waits River, and Gile Mountain Fms) and the light gray box indicates the Ordovician Moretown Fm. sample. The pressure break between Ordovician and CVT samples should be noted.

8–11 kbar going upgrade from the garnet zone west of the RMC to St–Ky zones at the Strafford Dome itself.

The main source of disagreement between QuiG barometry and the equilibrium-based methods was in

tSpear & Wolfe (2018) sample.

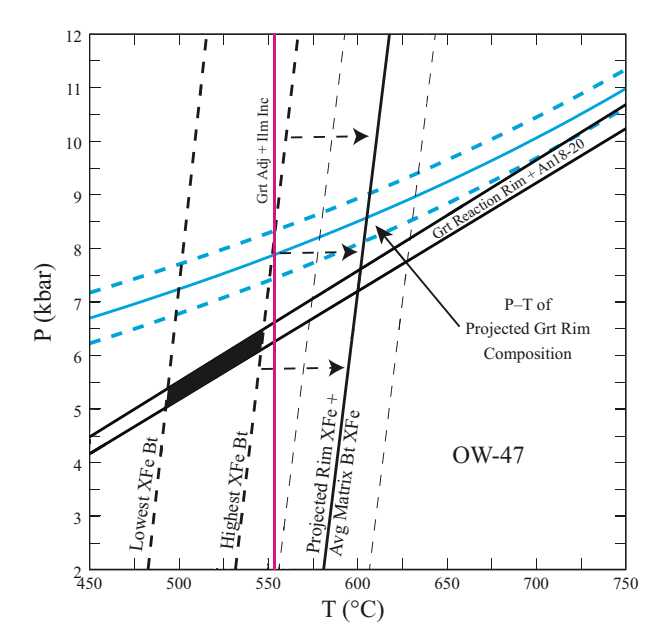


Fig. 10. P-T diagram for northern VT sample OW-47 showing QuiG and thermobarometry results (Grt–Bt, Grt–Ilm, and GPMB). It should be noted that the Grt–Bt thermometry lines as plotted in Fig. 7 are dashed (highest and lowest $X_{\rm Fe}$) because these mineral pairings result in temperature underestimates owing to the rim replacement and re-equilibration at lower T. The bold Grt–Bt curve is taken from the projected garnet composition inferred to have been present at the rim before garnet rim replacement by plagioclase occurred. The magenta vertical line shows the results from Grt–Ilm thermometry using an ilmenite inclusion within garnet. The black field shows the P-T conditions at which garnet replacement by plagioclase occurred.

determining initial garnet growth conditions and P-T paths from that information. As presented previously, both types of equilibrium calculations imply either unloading or loading P-T paths during garnet growth whereas QuiG barometry implies garnet growth at nearly constant P and T. Generally, loading paths have been inferred by many studies such as the near isothermal loading paths presented for several samples by Menard & Spear (1994). The comparison presented here suggests that prior P-T paths for the CVT determined using core-rim thermobarometry and/or garnet core isopleths might be in error. Spear et al. (2014) and Wolfe & Spear (2018) found similar disagreement between garnet growth conditions inferred from QuiG and garnet core equilibrium isopleths for similar rocks from central VT. Similar observations were also made by Castro & Spear (2017b) for rocks from the Cyclades blueschist belt in Sifnos, Greece. The interpretation of these studies, and the one favored here, is that garnet nucleated only after considerable overstepping of the equilibrium isograd and that the energy due to this overstepping that remained after nucleation provided the driving force for garnet growth at constant P and T. Therefore, we conclude that garnet core-to-rim conventional thermobarometry and garnet core intersecting isopleths did not reliably reveal the conditions of garnet growth for this suite of samples. There are isolated

examples where there was agreement (e.g. OW-19, OW-5C) between core thermobarometry and QuiG within uncertainty of both methods (± 1.0 kbar and ± 0.5 kbar respectively); however, these examples were not typical for this study. An analysis of the ramifications for classical thermobarometry of garnet nucleation after overstepping are beyond the scope of this paper but have been discussed by Spear & Wolfe (2018) and were examined in detail by Spear & Wolfe (2019). It is cautioned that there may be similar disagreement in P-T conditions determined by QuiG and garnet core thermobarometry or garnet core isopleths when applied to other terranes (e.g. Castro & Spear, 2017*b*; Catlos *et al.*, 2018; samples MA43, MA61, and MA65).

Applications of QuiG barometry and regional *P-T* trends

QuiG barometry presents an accessible and unique petrological tool to broadly characterize regional peak burial trends for a metamorphic terrane and mapped lithotectonic features such as the RMC and the sharp decrease in metamorphic grade observed east of the Strafford Dome in central VT (Doll et al., 1961; Spear et al., 2002). Overall, across the Goshen traverse, there is a modest decrease from east to west and Raman shifts of quartz inclusions generally fall in the range of 2.4-3.0 cm⁻¹ (Fig. 2b). Results can be broadly separated by the different formations where the samples were collected. Two of the Moretown Formation samples, OW-09 and OW-11, display the same maximum shift of 2.4 cm⁻¹. The Hawley Formation sample (OW-17), on the other hand, has a shift of 2.8 cm⁻¹, higher than that in the Moretown Formation. Samples from the Goshen Formation contain a range of shifts from 2.5 to 3.0 cm⁻¹ with most samples lying in the range of 2.8-3.0 cm⁻¹. The P-T conditions summarized in Fig. 8 show near complete overlap of QuiG and thermobarometry results, indicating similar peak metamorphic conditions across the RMC.

The central VT traverse samples display a range of shifts (Figs 2a and 9) from a low of 1.5 cm⁻¹ to a high of 3.5 cm⁻¹ with discontinuities in the amount of shift across the RMC (samples OW-5 and OW-1B) and east of the Strafford Dome (samples TM-549 and TM-551) (Fig. 2a; see also Spear et al., 2014). The discontinuity in Raman shifts on the east side of the map area coincides with the mapped decrease in metamorphic grade and depth of the CVT over the same distance (Doll et al., 1961). Samples from the western side of the Strafford Dome display Raman shifts in the range of 2.4–3.0 cm⁻¹ with no clear decreasing trend until the sharp drop at the RMC (dashed line in Fig. 2a; see Supplementary Data Fig S8 for finer scale geological map). West of the RMC, two samples, OW-1B and OW-5C, have maximum Raman shifts of 2.1 and 2.3 cm⁻¹, both less than the range of 2·7-3·0 cm⁻¹ recorded in adjacent Northfield Formation samples. This $\sim 0.5 \, \text{cm}^{-1}$ difference is consistent with some amount of offset across a syn- or

post-metamorphic fault coincident with the RMC. As shown in Fig. 9, this results in a \sim 1 kbar difference in peak pressure at similar temperatures across the RMC, and effectively an offset of \sim 3 km.

Samples from northern VT display a range of maximum Raman shifts of 1.2-2.0 cm⁻¹ (Figs 2c and 10). It is important to note that this section of the CVT has large mapped areas without observed garnet and thus a full traverse was not feasible in this locality. This range of inclusion shifts is lower than those from both the Goshen traverse and the western part of the central VT traverse and is similar to shifts observed in the lower garnet zone along the eastern margin of the central VT traverse. The lower range of Raman shifts is consistent with the overall decrease in metamorphic grade going north mapped by Doll et al. (1961), and with the northward shallowing of the CVT as recognized by the lowgrade chlorite, biotite and garnet zones in northern Vermont and Quebec (Thompson & Norton, 1968). In can be inferred that samples in northern VT reached peak pressure conditions at least \sim 1–2 kbar lower than equivalent St-Ky zone rocks in central VT and Goshen MA.

Application of QuiG barometry to the RMC resulted in mixed interpretations that mirror much of the conflicting literature concerning this contact (e.g. Hatch & Warren, 1981; Hatch & Stanley, 1988; Walsh et al., 2010). Classically, the RMC was inferred to be an unconformity between the Ordovician Rowe-Hawley belt and overlying Silurian-Devonian CVT (Richardson, 1919; White & Jahns, 1950; Doll et al., 1961; Hatch, 1969; Hatch et al., 1970; Menard & Spear, 1994). Later studies reinterpreted the RMC as a possible fault contact coincident with the RMC or a décollement (Hatch & Warren, 1981; Westerman, 1987; Hatch, 1988; Hatch & Stanley, 1988; Walsh et al., 2010). There is some indication that the peak pressures experienced by rocks to the west of the RMC from both traverses may be as much as 1 kbar lower than those to the east, but the differences are minor compared with the uncertainty in the calculations. If real, this difference indicates some minor late or post-metamorphic movement along this boundary. This interpretation is different from observations by Menard & Spear (1994), who interpreted a smooth metamorphic gradient across the RMC. A possible interpretation is that any movement of a possible fault or shear zone occurred before garnet growth, or the offset was not sufficiently great to be determined with thermobarometry given uncertainties in pressure estimates. Given the diverse textures and rock types observed around the RMC in the Goshen traverse, there may be additional P-T-t information to be found from other samples at this locality.

Where QuiG does reveal significant differences in metamorphic pressure is over the broad regional extent of the CVT from northern Vermont to western Massachusetts. Northern VT samples reached similar metamorphic grades (i.e. staurolite–kyanite zone metamorphism) and QuiG indicates pressure conditions at

least ~1–2 kbar lower than those for the other traverses to the south. This is entirely consistent with the mapped structure and isograds of the CVT (Thompson & Norton, 1968; Zen et al., 1983; Ratcliffe et al., 2011). Additionally, Raman shifts from samples east of the Strafford Dome in central VT reflect the dramatic decrease in *P*–*T* conditions from upper St–Ky zone to Chl zone. This trend was inferred to be due to postmetamorphic shortening during exhumation (Menard & Spear, 1994; Spear et al., 2002) and is reflected in the measured Raman shifts in garnet from this section of the central VT traverse.

CONCLUSIONS

Application of QuiG barometry has provided new insights and refinements to the interpretation of the metamorphism and the tectonic events associated with the Acadian Orogeny. The results of this study support the two main observations that were made by Wolfe & Spear (2018): that garnet appears to have nucleated at near peak P-T conditions and that the calculated equilibrium garnet-in curve was significantly overstepped in several instances. This is made more apparent when examining the MADs for each Goshen sample in Fig. 7. where QuiG never overlaps the intersection of the garnet core isopleths. Across both the Strafford and Goshen traverses, garnet core isopleths typically result in P-T conditions that are not reflected in QuiG barometry. This result indicates that it is not possible to constrain the prograde P-T path from garnet core isopleths when significant overstepping occurred. This is further coupled with the general observation that garnets in the CVT generally did not show any variation of Raman shifts with position within garnet, and thus garnet probably nucleates and grows at near isothermal-isobaric conditions, in effect requiring that P-T paths inferred from garnet zoning may need to be re-evaluated.

ACKNOWLEDGEMENTS

The authors would like to thank Adrian Castro and Karolina Kośmińska for assistance with sample collection, and Jared Singer for assistance with microprobe analyses. H. Stowell, D. Waters, A. van den Kerkhof, and J. Forshaw are gratefully acknowledged for their detailed reviews that helped improve this paper.

FUNDING

This research was funded by NSF grants 1321777 and 1447468 to F.S.S. and the Edward P. Hamilton Endowed Chair to F.S.S.

SUPPLEMENTARY DATA

Supplementary data are available at *Journal* of *Petrology* online.

REFERENCES

- Aleinikoff, J. N., Ratcliffe, N. M. & Walsh, G. J. (2011). Provisional zircon and monazite uranium-lead geochronology for selected rocks from Vermont. US Geological Survey Open-File Report 2011-1309.
- Angel, R. J., Alvaro, M., Miletich, R. & Nestola, F. (2017). A simple and generalised *P–T–V* EoS for continuous phase transitions, implemented in EosFit and applied to quartz. *Contributions to Mineralogy and Petrology* **172**, 29.
- Armstrong, T. R. & Tracy, R. J. (2000). One-dimensional thermal modelling of Acadian metamorphism in southern Vermont, USA. *Journal of Metamorphic Geology* **18**, 625–638.
- Armstrong, T. R., Tracy, R. J. & Hames, W. E. (1992). Contrasting styles of Taconian, eastern Acadian and western Acadian metamorphism, central and western New England. *Journal of Metamorphic Geology* **10**, 415–426.
- Ashley, K. T., Caddick, M. J., Steele-MacInnis, M. J., Bodnar, R. J. & Dragovic, B. (2014). Geothermobarometric history of subduction recorded by quartz inclusions in garnet. *Geochemistry, Geophysics, Geosystems* **15**, 350–360.
- Berman, R. G. (1988). Internally-consistent thermodynamic data for minerals in the system Na₂O-K₂O-CaO-MgO-FeO-Fe₂O₃-Al₂O₃-SiO₂-TiO₂-H₂O-CO₂. *Journal of Petrology* **29**, 445–522.
- Berman, R. G. (1990). Mixing properties of Ca–Mg–Fe–Mn garnets. *American Mineralogist* **75**, 328–344.
- Bayet, L., Agard, P., John, T., Menneken, M., Tan, Z. & Gao, J. (2019). Tectonic evolution of the Tianshan Akeyazi metamorphic complex (NW China). *Lithos* 354–355, 105273.
- Castro, A. E. & Spear, F. S. (2017a). Reaction overstepping and re-evaluation of peak *P*–*T* conditions of the blueschist unit Sifnos, Greece: implications for the Cyclades subduction zone. *International Geology Review* **59**, 548–562.
- Catlos, E. J., Lovera, O. M., Kelly, E. D., Ashley, K. T., Harrison, T. M. & Etzel, T. (2018). Modeling high-resolution pressure—temperature paths across the Himalayan main central thrust (Central Nepal): implications for the dynamics of collision. *Tectonics* 37, 2363–2388.
- Cheney, J. T. & Brady, J. B. (1992). Petrology of the high-alumina Hoosac schist from the chloritoid + garnet through the kyanite + biotite zones in Western Massachusetts. Guidebook for Field Trips in the Connecticut Valley Region of Massachusetts and Adjacent States 2, 332–357. Amherst, MA: Department of Geology and Geography, University of Massachusetts.
- Cheney, J. T., Spear, F. S. & Kirk-Lawlor, N. (2006). The mysterious machinations of muscovite and monazite during metamorphism or how the CVS (Connecticut Valley synclinorium) survived PMS (post-metamorphic stretching). *Geological Society of America Abstracts*, 38, 49.
- Dempster, T. J., La Piazza, J., Taylor, A. G., Beaudoin, N. & Chung, P. (2017). Chemical and textural equilibration of garnet during amphibolite facies metamorphism: The influence of coupled dissolution–reprecipitation. *Journal of Metamorphic Geology* 35, 1111–1130.
- Dempster, T. J., Gilmour, M. I. & Chung, P. (2019). The partial equilibration of garnet porphyroblasts in pelitic schists and its control on prograde metamorphism, Glen Roy, Scotland. *Journal of Metamorphic Geology* **37**, 383–399.
- Doll, C. G., Cady, W. M., Thompson, J. B., Jr & Billings, M. P. (1961). Centennial Geologic Map of Vermont, Scale: 1: 250,000. Montpelier: Vermont Geological Survey.
- Gatewood, M. P., Dragovic, B., Stowell, H. H., Baxter, E. F., Hirsch, D. M. & Bloom, R. (2015). Evaluating chemical equilibrium in metamorphic rocks using major element and Sm-Nd isotopic age zoning in garnet, Townshend Dam, Vermont, USA. Chemical Geology 401, 151–168.

- Graham, C. M. & Powell, R. (1984). A garnet-hornblende geothermometer: calibration, testing, and application to the Pelona Schist. *Journal of Metamorphic Geology* 2, 13–31.
- Guiraud, M. & Powell, R. (2006). *P–V–T* relationships and mineral equilibria in inclusions in minerals. *Earth and Planetary Science Letters* **244**, 683–694.
- Hames, W. E., Tracy, R. J. & Bodnar, R. J. (1989). Postmetamorphic unroofing history deduced from petrology, fluid inclusions, thermochronometry, and thermal modeling: an example from southwestern New England. *Geology* 17, 727–730.
- Hames, W. E., Tracy, R. J., Ratcliffe, N. M. & Sutter, J. F. (1991).
 Petrologic, structural, and geochronologic characteristics of the Acadian metamorphic overprint on the Taconide zone in part of southwestern New England. *American Journal of Science* 291, 887–913.
- Hatch, N. L., Jr. (1969). Geologic Map of the Worthington Quadrangle, Hampshire and Berkshire Counties, Massachusetts. US Geological Survey, Geologic Quadrangle Map GQ-857, Scale: 1:24,000. Reston, VA: US Geological Survey.
- Hatch, N. L., Jr (1988). Some revisions to the stratigraphy and structure of the Connecticut Valley trough, eastern Vermont. *American Journal of Science* **288**, 1041–1059.
- Hatch, N. L. & Stanley, R. S. (1988). Post-Taconian Structural Geology of the Rowe-Hawley Zone and the Connecticut Valley Belt West of the Mesozoic Basins. US Geological Survey Professional Paper 1366-C.
- Hatch, N. L., Jr & Warren, C. R. (1981). Geologic Map of the Goshen quadrangle, Franklin and Hampshire Counties, Massachusetts. US Geological Survey Geologic Quadrangle Map GQ-1561, Scale 1:24,000, http://pubs.er.usgs.gov/publi cation/gq1561.
- Hatch, N. L., Jr, Norton, S. A. & Clark, R. G., Jr (1970). Geologic Map of the Chester Quadrangle, Hampden and Hampshire Counties, Massachusetts. US Geological Survey Geologic Quadrangle Map GQ-858, Scale, 1:24,000. Reston, VA: US Geological Survey.
- Hemley, R. J. (1987). Pressure Dependence of Raman Spectra of SiO₂ Polymorphs: α-Quartz, Coesite, and Stishovite. In: Manghnani, M. H. & Syono, Y. (eds) *High-Pressure Research in Mineral Physics: A Volume in Honor of Syun-Iti Akimoto. American Geophysical Union, Geophysical Monograph* **39**, 347–359.
- Hibbard, J. P., Van Staal, C. R., Rankin, D. W. & Williams, H. (2006). Lithotectonic map of the Appalachian orogen, Canada–United States of America. Geological Survey of Canada, Map A, 2096, doi:10.4095/221912.
- Hillert, M. (2008). *Phase Equilibria, Phase Diagrams and Phase Transformations: Their Thermodynamic Basis.* Cambridge: Cambridge University Press.
- Hodges, K. V. & Crowley, P. T. (1985). Error estimation and empirical geothermobarometry for pelitic systems. *American Mineralogist* 70, 702–709.
- Hodges, K. V. & Spear, F. S. (1982). Geothermometry, Geobarometry and the Al_2SiO_5 Triple Point at Mt. Moosilauke, New Hampshire. *American Mineralogist* **67**, 1118–1134.
- Hollister, L. S. (1969). Contact metamorphism in the Kwoiek area of British Columbia: an end member of the metamorphic process. *Geological Society of America Bulletin* 80, 2465–2494.
- Kohn, M. J. (2014). "Thermoba-Raman-try": calibration of spectroscopic barometers and thermometers for mineral inclusions. Earth and Planetary Science Letters 388, 187–196.
- Kretz, R. (1983). Symbols for rock-forming minerals. *American Mineralogist* **68**, 277–279.

- Menard, T. & Spear, F. S. (1994). Metamorphic *P-T* paths from calcic pelitic schists from the Strafford Dome, Vermont, USA. *Journal of Metamorphic Geology* **12**, 811–826.
- Naylor, R. S. (1971). Acadian orogeny: an abrupt and brief event. *Science* **172**, 558–560.
- Palin, R. M., Weller, O. M., Waters, D. J. & Dyck, B. (2016). Quantifying geological uncertainty in metamorphic phase equilibria modelling; a Monte Carlo assessment and implications for tectonic interpretations. *Geoscience Frontiers* 7, 591–607.
- Pattison, D. R. & Tinkham, D. K. (2009). Interplay between equilibrium and kinetics in prograde metamorphism of pelites: an example from the Nelson aureole, British Columbia. *Journal of Metamorphic Geology* 27, 249–279.
- Pattison, D. R., De Capitani, C. & Gaidies, F. (2011). Petrological consequences of variations in metamorphic reaction affinity. *Journal of Metamorphic Geology* 29, 953–977.
- Peterman, E. M., Snoeyenbos, D. R., Jercinovic, M. J. & Kylander-Clark, A. (2016). Dissolution–reprecipitation metasomatism and growth of zircon within phosphatic garnet in metapelites from western Massachusetts. *American Mineralogist* 101, 1792–1806.
- Pownceby, M. I., Wall, V. J. & O'Neill, H. S. C. (1991). An experimental study of the effect of Ca upon garnet–ilmenite Fe–Mn exchange equilibria. *American Mineralogist* **76**, 1580–1588.
- Ratcliffe, N. M., Stanley, R. S., Gale, M. H., Thompson, P. J. & Walsh, G. J. (2011). Bedrock Geologic Map of Vermont. US Geological Survey Scientific Investigations Map 3184, 3 sheets, Scale 1:100,000. Reston, VA: US Geological Survey.
- Richardson, C. H. (1919). The Ordovician terranes of eastern Vermont. *Vermont State Geologist Report* 11, 45–51.
- Robinson, G. R., Jr. & Kapo, K. E. (2003). Generalized Lithology and Lithogeochemical Character of near-Surface Bedrock in the New England Region. US Geological Survey Open-File Report 03-225.
- Robinson, P., Tucker, R. D., Bradley, D., Berry, H. N., IV & Osberg, P. H. (1998). Paleozoic orogens in New England, USA. *GFF* 120, 119–148.
- Rosenfeld, J. L. (1969). Stress effects around quartz inclusions in almandine and the piezothermometry of coexisting aluminum silicates. *American Journal of Science* **267**, 317–351.
- Schmidt, C. & Ziemann, M. A. (2000). *In-situ* Raman spectroscopy of quartz: a pressure sensor for hydrothermal diamond-anvil cell experiments at elevated temperatures. *American Mineralogist* **85**, 1725–1734.
- Soret, M., Larson, K. P., Cottle, J. M., Smit, M., Johnson, A., Shrestha, S., Ali, A. & Faisal, S. (2019). Mesozoic to Cenozoic tectono-metamorphic history of the South Pamir–Hindu Kush (Chitral, NW Pakistan): insights from phase equilibria modelling, and garnet–monazite petrochronology. *Journal* of Metamorphic Geology 37, 633–666.
- Spear, F. S. & Menard, T. (1989). Program GIBBS: A FORTRAN Program for Gibbs Method Calculations. Troy, NY: Rensselaer Polytechnic Institute.
- Spear, F. S. & Pattison, D. R. (2017). The implications of overstepping for metamorphic assemblage diagrams (MADs). *Chemical Geology* **457**, 38–46.
- Spear, F. S. & Pyle, J. M. (2010). Theoretical modeling of monazite growth in a low-Ca metapelite. *Chemical Geology* 273, 111–119.

- Spear, F. S. & Wolfe, O. M. (2018). Evaluation of the effective bulk composition (EBC) during growth of garnet. *Chemical Geology* 491, 39–47.
- Spear, F. S. & Wolfe, O. M. (2019). Implications of overstepping of garnet nucleation for geothermometry, geobarometry and *P-T* path calculations. *Chemical Geology* **530**, 119323.
- Spear, F. S., Kohn, M. J., Cheney, J. T. & Florence, F. (2002). Metamorphic, thermal, and tectonic evolution of central New England. *Journal of Petrology* **43**, 2097–2120.
- Spear, F. S., Thomas, J. B. & Hallett, B. W. (2014). Overstepping the garnet isograd: a comparison of QuiG barometry and thermodynamic modeling. *Contributions to Mineralogy and Petrology* **168**, 1–15.
- Stanley, R. S. & Hatch, N. L., Jr (1988). The Pre-Silurian Geology of the Rowe-Hawley Zone. The Bedrock Geology of Massachusetts. US Geological Survey Professional Paper 1366. A1–A39.
- Thomas, J. B. & Spear, F. S. (2018). Experimental study of quartz inclusions in garnet at pressures up to 3·0 GPa: evaluating validity of the quartz-in-garnet inclusion elastic thermobarometer. *Contributions to Mineralogy and Petrology* 173, 1–14.
- Thompson, J. B., Jr & Norton, S. A. (1968). Paleozoic regional metamorphism in New England and adjacent areas. In: Zen, E-ari, White, W. S., Hadley, J. B., & Thompson, J. B., Jr., (eds) Studies in Appalachian Geology: Northern and Maritime. New York, Interscience Publishers, pp. 319–327.
- Tinkham, D. K. & Ghent, E. D. (2005). Estimating *PT* conditions of garnet growth with isochemical phase-diagram sections and the problem of effective bulk-composition. *Canadian Mineralogist* **43**, 35–50.
- Vance, D. & Holland, T. (1993). A detailed isotopic and petrological study of a single garnet from the Gassetts Schist, Vermont. Contributions to Mineralogy and Petrology 114, 101–118.
- Viete, D. R., Hacker, B. R., Allen, M. B., Seward, G. G. E., Tobin, M. J., Kelley, C. S., Cinque, G. & Duckworth, A. R. (2018). Metamorphic records of multiple seismic cycles during subduction. *Science Advances* 4, eaaq0234.
- Walsh, G. J., Kim, J., Gale, M. H. & King, S. M. (2010). *Bedrock Geologic Map of the Montpelier and Barre West Quadrangles, Washington and Orange Counties, Vermont.*Reston, VA: US Geological Survey.
- Westerman, D. S. (1987). Structures in the Dog River fault zone between Northfield and Montpelier, Vermont. In: Westerman D. S. (ed.) Guidebook for Field Trips in Vermont: New England Intercollegiate Geological Conference, 79th Annual Meeting, Montpelier, Vermont, Vol. 2, pp. 109–132. Department of Earth Science Norwich University Northfield, VT.
- White, W. S. & Jahns, R. H. (1950). Structure of central and east–central Vermont. *Journal of Geology* **58**, 179–220.
- Wolfe, O. M. & Spear, F. S. (2018). Determining the amount of overstepping required to nucleate garnet during Barrovian regional metamorphism, Connecticut Valley Synclinorium. *Journal of Metamorphic Geology* **36**, 79–94.
- Zen, E.-A., Goldsmith, R., Ratcliffe, N. M., Robinson, P., Stanley, R. S., Hatch, N. L., Shride, A. F., Weed, E. G. A. & Wones, D. R. (1983). Bedrock Geologic Map of Massachusetts. US Geological Survey. Scale 1:250 000. Reston, VA: US Geological Survey.